Coupled K^+–Water Flux through the HERG Potassium Channel Measured by an Osmotic Pulse Method

Hiroyuki Ando,[1,4] Miyuki Kuno,[3] Hirofumi Shimizu,[1,2] Ikunobu Muramatsu,[4] and Shigetoshi Oiki[1,2]

[1]Department of Molecular Physiology and Biophysics, University of Fukui Faculty of Medical Sciences, Fukui 910-1193, Japan
[2]CREST, Japan Science and Technology Agency, Saitama 332-0012, Japan
[3]Department of Physiology, Osaka City University Graduate School of Medicine, Osaka 545-8585, Japan
[4]Department of Pharmacology, University of Fukui Faculty of Medical Sciences, Fukui 910-1193, Japan

The streaming potential (V_{stream}) is a signature feature of ion channels in which permeating ions and water molecules move in a single file. V_{stream} provides a quantitative measure of the ion and water flux (the water–ion coupling ratio), the knowledge of which is a prerequisite for elucidating the mechanisms of ion permeation. We have developed a method to measure V_{stream} with the whole-cell patch-clamp configuration. A HEK293 cell stably expressing the HERG potassium channel was voltage clamped and exposed to hyperosmotic solutions for short periods of time (<1 s) by an ultrafast solution switching system (the osmotic pulse [quick jump-and-away] method). The reversal potentials were monitored by a series of voltage ramps before, during, and after the osmotic pulse. The shifts of the reversal potentials immediately after the osmotic jump gave V_{stream}. In symmetrical K^+ solutions (10 mM), the V_{stream}s measured at different osmolalities showed a linear relationship with a slope of −0.7 mV/ΔOsm, from which the water–ion coupling ratio (n, the ratio of the flux of water to the flux of cations; Levitt, D.G., S.R. Elias, and J.M. Hautman. 1978. *Biochim. Biophys. Acta.* 512:436–451) was calculated to be 1.4. In symmetrical 100 mM K^+ solutions, the coupling ratio was decreased significantly (n = 0.9), indicating that the permeation process through states with increased ion occupancy became significant. We presented a diagrammatic representation linking the water–ion coupling ratio to the mode of ion permeation and suggested that the coupling ratio of one may represent the least hydrated ion flux in the single-file pore.

INTRODUCTION

Electroosmosis is a natural consequence of ion permeation through channels; in the presence of a concentration gradient or potential difference across a membrane, ions permeating through the pore are accompanied by water molecules. Conversely, an osmotic gradient across the membrane produces a flux of water that carries ions through the pore even in the absence of an electrochemical potential difference; this flux generates a streaming potential (V_{stream}; Katchalsky and Curran, 1965). V_{stream} has been used to establish that permeating ions pass through an aqueous pore (Finkelstein and Andersen, 1981; Hille, 2001) and to infer the structural features of ion channels in the presence of a single-file regime (Levitt et al., 1978; Rosenberg and Finkelstein, 1978; Miller, 1982; Alcayaga et al., 1989; Dani, 1989; Tu et al., 1994; Ismailov et al., 1997; Tripathi and Hladky, 1998). We extended here the use of V_{stream} by developing a method for measuring V_{stream} from the whole-cell recordings. Then, by revisiting a relationship that V_{stream} derives (Levitt et al., 1978), the permeation mode, in which ions and water molecules are transferred, was inferred from measured V_{stream}.

Recently the high-resolution crystal structure of a potassium channel, KcsA, has revealed a single-file nature of the selectivity filter and the distribution of ions and water molecules in the pore (Zhou et al., 2001; Zhou and MacKinnon, 2003; Fig. 1 A). These static pictures were mobilized by computational methods, in which ions and water molecules were transferred in a concerted manner (Chung et al., 1999; Guidoni et al., 2000; Berneche and Roux, 2001; Luzhkov and Aqvist, 2001). This supports the old idea that K^+ permeates in a single file through the selectivity filter of potassium channels. A new permeation model has been proposed (Fig. 1 B; Morais-Cabral et al., 2001), in which the states of K^+–water distribution in the selectivity filter and the transitions linking them are shown (here we call this the shift-permeation model). This model poses a general framework for understanding permeation characteristics of potassium channels in general. Electrophysiologically, single-channel current recordings of KcsA channels show a nonsaturable concentration–current relationship (Zhou et al., 2001). This was simulated by the shift-permeation model with a preferential mode of transition between i-w-i-w and w-i-w-i through the transition state of i-w-i-w-i (the top triangle in Fig. 1 B; i, ion; w, water molecule). These studies have provided a solid basis for understanding the mechanism of ion permeation through potassium channels but need further experimental supports.

Correspondence to Shigetoshi Oiki: oiki-fki@umin.ac.jp

J. Gen. Physiol. © The Rockefeller University Press $8.00
Volume 126 Number 5 November 2005 529–538
http://www.jgp.org/cgi/doi/10.1085/jgp.200509377

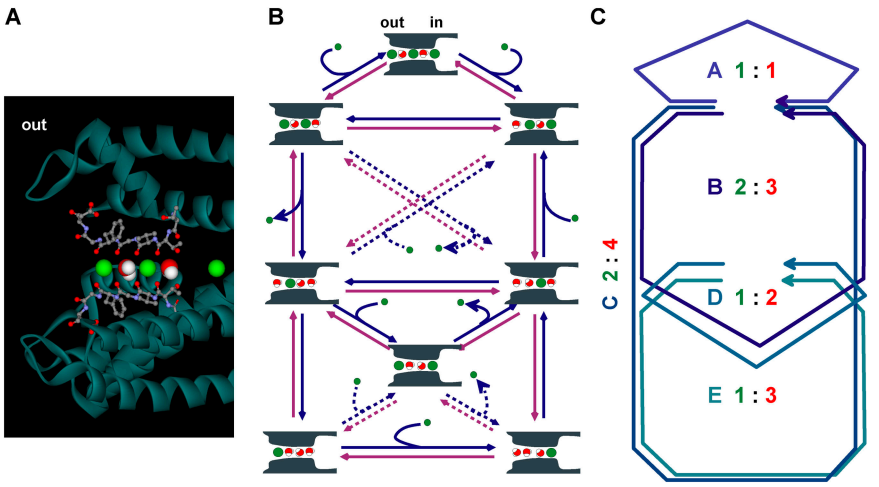

Figure 1. Permeation of K^+ and water molecules through potassium channels. Green, potassium ion; red, water molecule. (A) A distribution of K^+ and water molecules in the pore of the KcsA channel. The single-file nature of K^+ and water molecules is seen in the selectivity filter. The selectivity filter is shown by the ball-and-stick model. (B) The simplified shift-permeation model for K^+ and water permeation through a K^+-selective pore (left side, extracellular). Each cartoon represents a K^+–water-occupied state in the selectivity filter. Arrows indicate transitions between states, which accompany shift movements of ion–water columns. Blue arrows indicate transitions for efflux; purple arrows for influx. Curved arrows indicate K^+ entering or exiting from the selectivity filter. Arrows representing the exchange transitions, in which K^+ and a water molecule exchange at either end of the filter and no shift movements accompany, are shown by broken lines. (C) A cycle flux diagram. Each cycle was drawn by connecting states, by completing a cycle, net movements of ion and water were performed. For each cycle, the ratio of coupled transport of K^+ and water molecules (K^+ [green number]: water molecules [red number]) is indicated (the coupling ratio = water/K^+). For example, the cycle A exhibits the coupling ratio of one; the cycle C and D show the coupling ratio of two. At low K^+ concentrations, the probability being in cycles at lower positions, such as in cycle D and E, is high. As K^+ concentration increases, cycle fluxes at upper positions become predominant. Cycle fluxes with exchange transitions are not shown.

In this study permeation characteristics of the HERG potassium channel (*KCNH2*; Trudeau et al., 1995) was investigated by measuring V_{stream}. The selectivity filter of the potassium channel gene family is highly homologous in its sequence and the family members are closely similar in structure (Jiang et al., 2002, 2003; Kuo et al., 2003; Long et al., 2005). Therefore, the ion permeation through the selectivity filter of HERG channels should be single file in nature. Unlike other potassium channels, however, the signature sequence of the selectivity filter of HERG channel is G-F-G rather than G-Y-G, and this difference has not yet been related to its permeation features. By measuring V_{stream} at different potassium concentrations the water–ion coupling ratio (the ratio of the flux of water to the flux of cations) was evaluated. This value can be related to the mode of ion permeation (Fig. 1 C). Despite its effectiveness, difficulties in measuring V_{stream} have limited the use of the coupling ratio. Therefore a rapid and simple measurement of V_{stream} is highly desirable. We present here an osmotic pulse method for accurate evaluation of V_{stream} under the voltage-clamped whole-cell recordings.

MATERIALS AND METHODS

Cell

The HEK293 cells were transfected with HERG cDNA (a gift from G.A. Robertson, University of Wisconsin, Madison, WI) using lipofectamine 2000 (Invitrogen). After selection in 800 μg/ml Geneticin (G-418, Invitrogen) for 15–20 d, single colonies were picked with cloning cylinders and tested for HERG currents. The stably transfected cells were cultured in Dulbecco's modified Eagle's medium (DMEM) supplemented with 10% FBS and 400 μg/ml G-418. All cells were from a single cell line producing high current levels and were stable for 3 mo or more. For electrophysiological studies, the cells were harvested from the culture dish by trypsinization, washed with DMEM, and stored in this medium at room temperature for later use. Cells were studied within 5 h of harvest.

Multibarreled Tube

A triple-barreled tube was fabricated from stainless steel needles (19 G, 10 cm) bundled in parallel with epoxy resin (Fig. 2 A). At the tips of the metal tubes, fine fused silica tubes coated with polyimide (MicroFil, WPI) were inserted to define a small tip of fixed size (the inner diameter of the tip is 250 μm; the length is 10 mm) for the outlet. The solution flows were controlled independently by an injection pump (TE-221, Terumo). Parallel laminar flows with clear interface were visible under microscope (Fig. 2 B). The bath solutions (iso-osmotic solutions identical with those for the tube) were also perfused with the flow rate of 0.8 ml/min.

Ultrafast Solution Exchange

To circumvent adverse cellular responses upon osmotic shock, an osmotic pulse method was used by which patch-clamped cells were exposed to the osmotic gradient briefly. An ultrafast switching system (LSS-3200, EXFO) was used for quick solution changes. The movement of the piezoelectric device (the movement range: 200 μm) was triggered from the pulse protocol in the pClamp software. To eliminate the mechanical oscillations of the tubes and the subsequent undulations of flow upon shift movements, the driving voltage (5 V) for the piezoelectric device was started and terminated with a finite slope. A patch-clamped cell was placed in the outflow of the central tube (the iso-osmotic solution; Fig. 2 C). Dumped movements of the triple-barreled tube lead smooth transfer of the laminar flows and the cell was subjected to cross the interface without disturbance. After returning to the iso-osmotic solution, differences in the cell appearance and changes in the cell size were not detected. The patch-clamped cell survived in repeated exposures to the hyperosmotic solution, thus, different osmotic solutions, using triple-barreled tube, could be examined in a single cell.

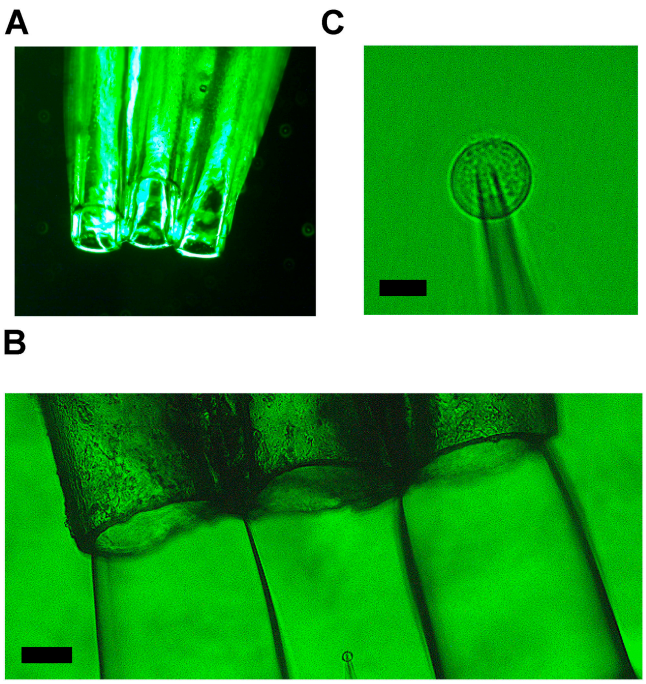

Figure 2. The jump-and-away system. (A) A triple-barrel tube. Only a part of the tip is shown. (B) A triple-barrel tube (top) and a patch-clamped cell (bottom). The inner diameter of the tube is 250 μm. Center outflow, the iso-osmotic solution. The patch-clamped cell was placed in the midst of the flow of the iso-osmotic solution (the flow rate was 0.07–0.08 ml/min). Left and right outflows, the hyperosmotic solutions (1,000 and 1,500 mOsm). (C) A patch-clamped HEK293 cell under flow. The scale bars are 100 μm and 10 μm for B and C, respectively.

Electrophysiology

Whole-cell recordings were performed with an amplifier (Axo-Patch 200B, Axon Instruments). Currents were filtered at 1 kHz and sampled at 10 kHz with DigiData1322A (Axon Instruments). The extracellular solution contained (in mM) 100 or 10 KCl, 1.8 $CaCl_2$, 1.0 $MgCl_2$, 60 or 150 NMDG, and 10 HEPES (pH 7.4 with HCl). The pipette solutions were 100 or 10 KCl, 2.0 $MgCl_2$, 5.0 EGTA, 50 or 140 NMDG, 5.0 MgATP, and 10 HEPES (pH 7.2 with HCl). Perfusing solutions with the same ionic composition but with different osmolalities (concentrations are on a molal basis; mol/kg H_2O) were prepared using sorbitol. The osmolalities were measured with an osmometer (Osmostat OM-6040 Arkray). Pipette resistances were 2–4 MΩ. The series resistance was not compensated. A ramp command contained both depolarizing (from −20 mV to +20 mV) and hyperpolarizing (from +20 mV to −20 mV) branches with the whole time course of 16 ms. A series of 10 or 26 ramps were applied: one before the depolarizing pulse (preactivation ramp) and 9 or 25 during steady inward current recordings (activation ramp). The preactivation ramps were preceded by a brief depolarization pulse (10 ms) to eliminate the large capacitative currents at the beginning of the ramp. During 9 or 25 active ramps (interval: 150 ms) a brief osmotic pulse (380 ms or less) was applied. All experiments were performed at room temperature (23°C).

Numerical Evaluation of V_{rev}

To evaluate V_{rev} precisely from the macroscopic current recordings, the errors arising from the series resistance for estimating real membrane voltages were avoided. The current traces during a ramp command (both depolarizing and hyperpolarizing branches of the current trace) were fitted. The currents through an equivalent membrane circuit driven by the same ramp command were simulated and the parameters of the circuit were optimized to fit the recorded currents. The equivalent membrane circuits included the reversal potential (V_{rev}), series resistance (R_a), membrane conductance ($G_m = 1/R_m$), leak resistance (R_s), and membrane capacitance (C_m) as free parameters. For the determination of R_s and C_m, the current traces elicited by the preactivation ramp were fitted. Using these parameters the activation ramp currents were fitted for the rest of the parameters. To represent the time dependence of the channel conductance during the ramp, linear changes in the conductance were introduced, such that $g_m(t) = G_m \times (a\ t + b)$. The coefficients ($a$, b) were set separately for either the depolarizing or hyperpolarizing branches of the ramp command and were kept fixed throughout a train. Numerical integration of the differential equation for the equivalent circuit was performed (Mathematica ver. 5.0, Wolfram) and the parameters were optimized using the Nelder-Mead algorithm.

The Shift of V_{rev} and V_{stream}

V_{stream} was measured as the shift of V_{rev} upon establishment of an osmotic gradient (ΔV_{rev}) but in our experimental configuration the following factors must be subtracted from the ΔV_{rev} values. For different osmotic solutions the activities of K^+ are different even if the molality is the same (Levitt et al., 1978). Therefore, the shift of the equilibrium potential for K^+ (E_K) arises upon exposure to the hyperosmotic solution across the HERG channel-expressing, potassium-selective membrane. This shift of E_K was evaluated by a K^+-selective electrode (Orion 97–19 ionplus Potassium Electrode; Thermo Electron Corporation) as the difference of measured potentials between the iso- and hyperosmotic solutions, which is expressed in mV ($\Delta V_{activity}$). At the same time, the differences in the electrolyte activity between different osmotic solutions generate a liquid junction potential (V_{LJ}). In our experimental configuration V_{LJ} arose at the interface between the laminar outflows of hyperosmotic solution and the bathing (iso-osmotic) solution (see DISCUSSION). V_{LJ} was measured by an open-tip electrode under the current-clamp mode, during which a pressure was applied to the pipette so as not to mix the flowing solutions with the pipette solutions (3 M KCl). From the physicochemical point of view, V_{stream} was thus defined as $V_{stream} = \Delta V_{rev} - \Delta V_{activity} - V_{LJ}$, in which propagation of errors was taken into account.

The measurements of V_{LJ} were also used for evaluating the time course of the osmotic jump. The time constant of the jump was <1 ms, indicating that the osmotic clamp was performed instantaneously. Data are shown as mean ± SEM.

RESULTS

HERG Current and Osmotic Pulse

Since the formulation of irreversible thermodynamics requires near-equilibrium conditions, the experimental solutions were symmetric in terms of the K^+ concentrations (100 mM). The typical currents of the HERG potassium channels expressed in HEK293 cells displayed an activation at +20 mV followed by large inward tail current at negative potentials (Fig. 3 A). The presence of the HERG-specific blocker, E-4031, depressed the tail current markedly (Fig. 3 B). The current–voltage curves (*I-V* curves) at 50 ms after the repolarizing steps (Fig. 3

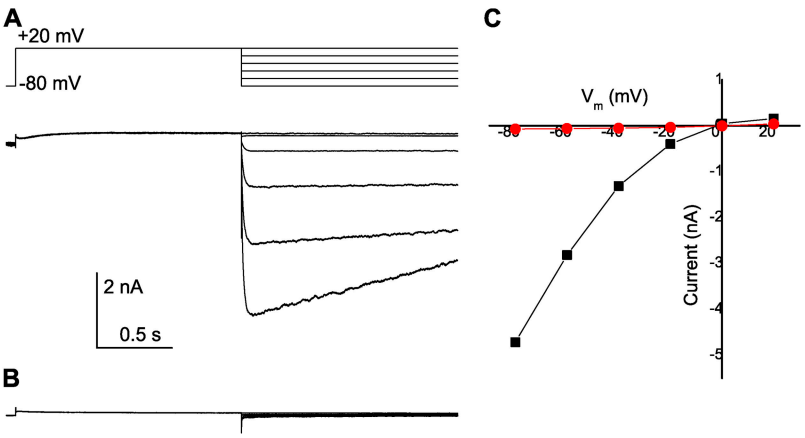

Figure 3. HERG current expressed in HEK293 cells. (A) Tail current recordings at different potentials. Currents were elicited by depolarizing pulses at +20 mV followed by hyperpolarizing pulses (from 0 to −80 mV). (B) Currents remaining after treatment with 10 μM E-4031. (C) Current–voltage curves of tail currents before (black symbols) and after (red symbols) the treatment of E-4031 measured at 50 ms after the steps to repolarizing potentials.

C) are shown. The *I-V* curve with the blocker indicated that contributions from other currents were negligible.

With relatively long lasting voltage commands, the inward currents recorded at −20 mV were nearly steady (Fig. 4 A) since the open probability was maximal and the deactivation process was very slow at that voltage. Returning to the holding potential of −80 mV elicited large inward currents followed by a slow deactivation. In the presence of the blocker (the violet trace), the current amplitude at –20 mV was negligible. Trains of ramp voltages were delivered at −20 mV at intervals of 150 ms, and during the middle of a train of nine ramps (from 4 to 6) an osmotic pulse of 380 ms was applied. The inward currents (amplified in Fig. 4 B) were depressed slightly during the pulse, indicating the effects of the quick exposure to the hyperosmotic solution.

With ramps consisting of depolarizing (8 ms) and hyperpolarizing (8 ms) arms between −20 to +20 mV,

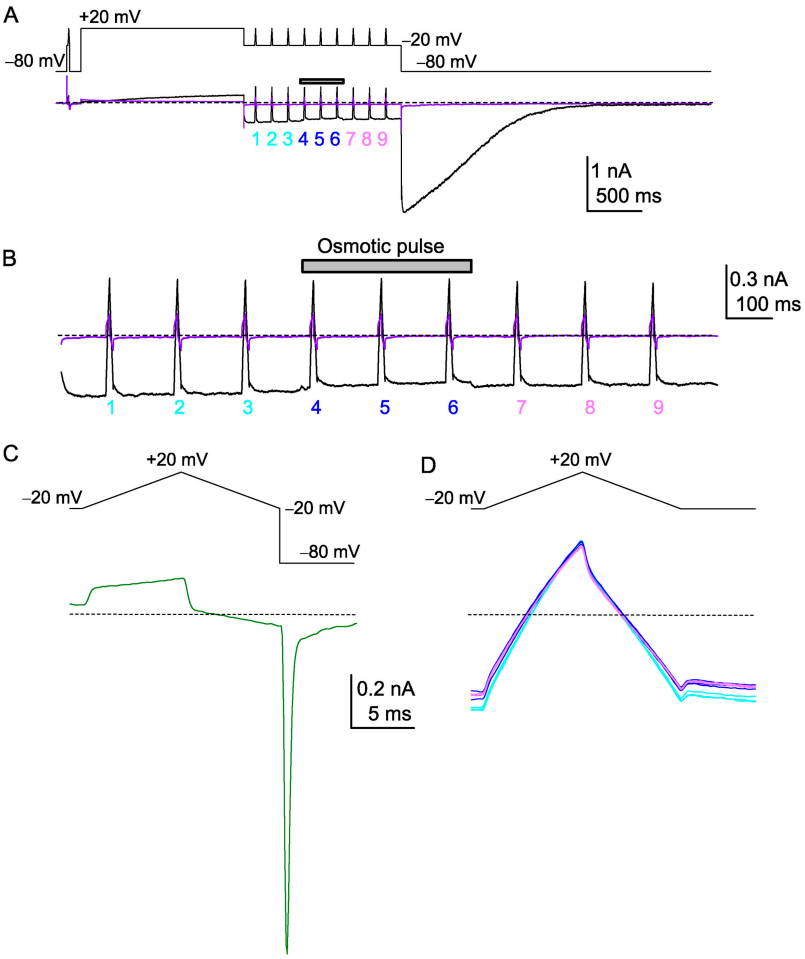

Figure 4. HERG current recordings and the osmotic pulse. (A) The time course of the current recording in symmetrical 100 mM K^+ solution. Top, voltage protocol; Bottom, current traces. Preactivation ramp command: prior to the long depolarization pulse, a brief prepulse to −20 mV followed by a depolarization–repolarization ramp was applied. Activation ramp command: nine ramp commands were delivered at −20 mV (numbering 1 to 9). The osmotic pulse (380 ms, 1000 mOsm) was applied from just before the 4 ramp to just after the 6 ramp. Current trace in violet color indicates recordings after the treatment of E-4031. (B) A train of the ramp currents with an expanded time scale. An osmotic pulse induced a slight depression of the inward current. (C) A current trace (bottom) for the preactivation ramp command (top). (D) Current traces (bottom) for the activation ramp command (top) before (light blue), during (dark blue), and after (light purple) the osmotic pulse. Broken lines indicate the zero current level.

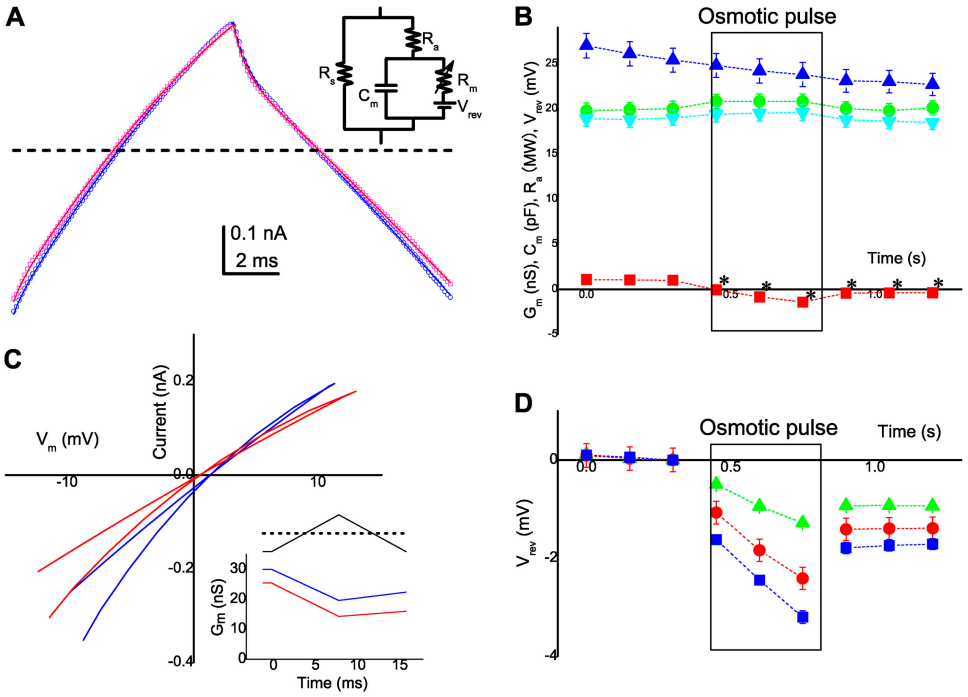

Figure 5. The evaluation of V_{rev}. (A) Recorded ramp currents (open symbols) just before an osmotic pulse (3; blue) and the first one during the osmotic pulse (4; red; 1,000 mOsm). The current through the equivalent membrane circuit (inset, the variable membrane resistance [R_m], the membrane capacitance [C_m], the series resistance [R_a], and the seal resistance [R_s]) for the ramp command was simulated. The free parameters (V_{rev}, G_m [$= 1/R_m$], R_a, and C_m) were optimized and the fitted curves were superimposed on the recorded currents. (B) The time course of changes in the fitted parameters during a train. ▲, G_m (nS); ●, R_a (MΩ); ▼, C_m (pF); ■, V_{rev} (mV). The starting time for the first ramp (1) was set to zero. The pulse duration was boxed, starting from 440 ms and ending at 820 ms. The first ramp during the pulse (4) was applied immediately (<10 ms) after the jump. For V_{rev}, error bars were within the sizes of the symbols and the asterisks indicate statistical significance ($P < 0.05$). (C) *I-V* curves reconstructed from the fitted parameters for the current traces in A. Current amplitudes were calculated as $(V_{memb}[t] - V_{rev}[t]) \times G_m(t)$ and plotted as a function of $V_{memb}[t]$. All the values are time-based variables and a parametric plot was performed. Inset, the ramp command and the time course of the membrane conductance. The conductance changes were correlated to the time course of the ramp command. The slopes of the conductance changes were optimized. (D) The time courses of V_{rev} changes for different osmolalities. ▲, 500 mOsm; ●, 1000 mOsm; and ■, 1500 mOsm. The V_{rev} values were normalized by the values for ramp 3.

the resulting current traces elicited before the activation of the HERG channel (the preactivation ramp currents) (Fig. 4 C) were used to evaluate the seal resistance and the membrane capacitance. The activation ramp current during recording of the activated HERG channel showed an initial capacitive jump followed by a slightly curved time course (Fig. 4 D). This weak "rectification," even during voltage sweeps between −20 and +20 mV as fast as 8 ms, was the result of the fast inactivation of the HERG channel. When the depolarizing and hyperpolarizing branches of a current trace in the time domain were folded, the absence of overlap reflected the asymmetrical time course of the gating.

Shifts of V_{rev} upon the Osmotic Pulse

The ramp currents before (blue) and during (red) the osmotic pulse showed little difference and did not readily display visible shifts in V_{rev} (Fig. 5 A). To evaluate the shift accurately, the activation ramp currents were fitted with an equivalent membrane model, in which time-dependent conductance changes in the channel currents were incorporated (Fig. 5 A, inset; see MATERIALS AND METHODS in detail). This nonlinear implementation, introduced here first, turned out to give reliable and reproducible estimates of V_{rev} within 0.02 mV.

The most prominent changes in the membrane parameters and in their time courses during a train of ramp commands (Fig. 5 B) were seen in V_{rev}. In addition, the membrane conductance decreased gradually as a consequence of the deactivating currents. The other parameters were not changed significantly. The *I-V* curves reconstructed from the fitted parameters (Fig. 5 C) showed faster inactivation in the depolarizing branches and slower de-inactivation in the hyperpolarizing branches, that is hysteresis. It should be noted that the depolarizing and hyperpolarizing branches cross at V_{rev}, meaning that the hysteresis did not affect the estimation of V_{rev}.

Successive Monitorings of V_{rev} Revealed Condensation of $[K^+]_i$

The time courses of V_{rev} for different osmolalities (Fig. 5 D) show V_{rev} to be stable before the osmotic pulses (1 to 3). V_{rev} jumped to negative potentials at the onset of the osmotic pulse and continued to shift throughout the duration of the pulse (4 to 6). The slope of the V_{rev} shift during the pulse increased with increasing osmolality. After the return to the iso-osmotic solution, V_{rev} did not recover to the original level immediately (7 to 9) and it stayed at the negatively shifted level for seconds (for the subsequent recovery see APPENDIX).

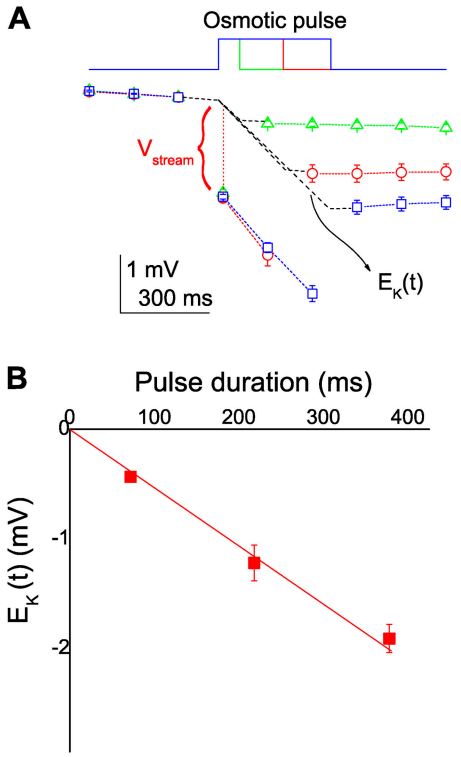

Figure 6. (A) Time courses of V_{rev} for osmotic pulses with different durations. V_{rev} values for each train were normalized by the value of prepulse (3). Osmotic pulses of 1,500 mOsm were applied for 75, 230, or 380 ms, during which one, two, or three ramps were delivered. The time courses of $E_K(t)$ during a pulse was drawn as a broken line through interpolation from the start of the osmotic pulse to the end of the pulse. (B) The V_{rev} value on return to the iso-osmotic solution (E_K) as a function of the pulse duration.

In the absence of osmotic gradients, V_{rev} represents the equilibrium potential for K^+ (E_K). Thus, the significant shifts of E_K before and after the pulse indicate changes in the intracellular K^+ concentrations ($[K^+]_i$), since the cell was perfused continually, and consequently local concentration changes did not develop outside the cell near the membrane. The negative shifts of E_K represent condensation of $[K^+]_i$ as a result of water depletion through the osmotically driven efflux. The E_K values after different osmotic pulses indicate that $[K^+]_i$ were more condensed during exposures to higher osmotic gradients. Visual inspection did not detect changes in the cell size before and after the pulse.

Upon the osmotic pulses, V_{stream} should rise immediately, since the osmotic gradient was applied in a stepwise fashion (see MATERIALS AND METHODS). On the other hand, water depletion in the cell during a pulse led to a slowly developing condensation of $[K^+]_i$. Thus, the changes in V_{rev} included the time-invariant V_{stream} and the slow shift in E_K. To extract the V_{stream} values from the changes in V_{rev}, the underlying time courses of the E_K shift during the pulse must be observed. The duration of the osmotic pulse was shortened and the E_K on return to the iso-osmotic solution was measured (Fig. 6 A). The negative shift of the value of E_K was less with shorter pulses. The plot of the first V_{rev} values on return to the iso-osmotic solution (or E_K) as a function of the pulse duration (Fig. 6 B) showed a linear relationship. This observed linearity in E_K reflected the underlying time course in E_K during the pulse, which was rewritten as $E_K(t)$ and is shown as a broken line in Fig. 6 A. Hereafter the linear time courses of $E_K(t)$ during the osmotic pulses were used for estimating the V_{stream} values.

TABLE I

Differences of K^+ Activities and the Liquid Junction Potentials between Hyperosmotic Solutions and the Iso-osmotic Solution

	100 K (mV)		10 K (mV)	
ΔOsm (mOsm)	$\Delta V_{activity}$	V_{LJ}	$\Delta V_{activity}$	V_{LJ}
500	−0.34 ± 0.05	−0.06 ± 0.01	−0.18 ± 0.05	−0.12 ± 0.03
1,000	−0.50 ± 0.04	−0.08 ± 0.01	−0.45 ± 0.07	−0.32 ± 0.02
1,500	−0.75 ± 0.07	−0.18 ± 0.02	−0.83 ± 0.06	−0.43 ± 0.01

V_{stream} for Different Osmolalities and K^+ Concentrations

V_{rev} during the pulses seemed to change in parallel with $E_K(t)$. The first values of V_{rev} for different-duration pulses overlapped (Fig. 6 A). Thus we used the V_{rev} values immediately after the jump as the most reliable estimates for V_{stream}. The graphical representation shows V_{stream} as a vertical distance between V_{rev} (symbols during the pulse) and $E_K(t)$ (broken lines). Finally, the precise values of V_{stream} were evaluated through subtracting the measured values of V_{LJ} and $\Delta V_{activity}$ (Table I) from the vertical distances.

A plot of values of V_{stream} for symmetrical 100 mM K^+ solutions as a function of the osmolality (Fig. 7) showed a linear relationship with a slope of −0.4 mV/ΔOsm. From the equation (Levitt et al., 1978; Rosenberg and Finkelstein, 1978) $\Delta\Psi/\Delta\pi = -nv_w/zF$, n, the ratio of the water flux to the K^+ flux, was determined to be 0.9 ($\Delta\Psi$, V_{stream}; $\Delta\pi$, the osmotic pressure; v_w, the molar volume of water; z, the valence of K^+; F, the Faraday constant). This value represents the least hydrated K^+ transfer in the single-file pore.

In lower K^+ concentrations, the number of occupied potassium ions in the selectivity filter should decrease and the coupling ratio would be expected to increase (Fig. 1). V_{stream} was measured in symmetrical 10 mM K^+ solutions. The current traces for a ramp exhibited more rectification than those for the high K^+ condition (unpublished data), indicating faster inactivation at lower K^+ solutions, i.e., a typical feature of the HERG channel (Shimizu et al., 2003). In the low K^+ solutions the values of V_{LJ} were augmented (Table I). The V_{stream} values for symmetrical 10 mM K^+ solutions demonstrated a linear relationship (Fig. 7). The coupling ra-

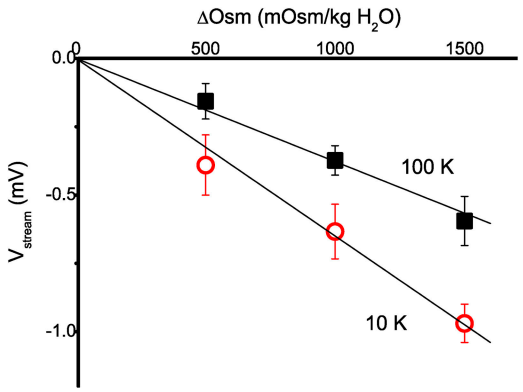

Figure 7. V_{stream} and its osmolality dependency. V_{stream} as a function of the osmolality. Linear fits with slopes of −0.4 mV/ΔOsm and −0.7 mV/ΔOsm were obtained for 100 mM and 10 mM K^+.

tio was determined to be 1.4, which is significantly higher than those in the higher K^+ concentrations.

DISCUSSION

We have developed an efficient and reproducible method to evaluate V_{stream} using the voltage-clamp whole-cell recordings. In this study, the V_{stream} for the HERG potassium channel expressed in HEK293 cells was investigated in different osmolalities and K^+ concentrations. Values of V_{stream} as small as −0.4 mV could be detected in this method, and the value of n, the ratios of the water flux to the K^+ flux, were evaluated.

First, methodological issues will be discussed. In the procedures used here, the repeated application of different hyperosmotic solutions to a single cell can be performed, which enhanced the efficiency and accuracy of the measurements. This method, with macroscopic current measurements, can be applied to channels with conductances too small to resolve.

Two problems inherent in the current recordings from patch-clamped cells had to be solved to develop the method. First, to circumvent adverse cellular responses upon osmotic shock, a method was developed to expose a patch-clamped cell to brief osmotic pulses. This quick jump method in combination with the voltage-clamped configuration provided additional benefits for obtaining more reliable recordings. Stepwise changes of osmolality and immediate measurements of the shift of V_{rev} within a few milliseconds enabled the detection of the rapid responses of the channel pore per se. This method minimized possible contamination

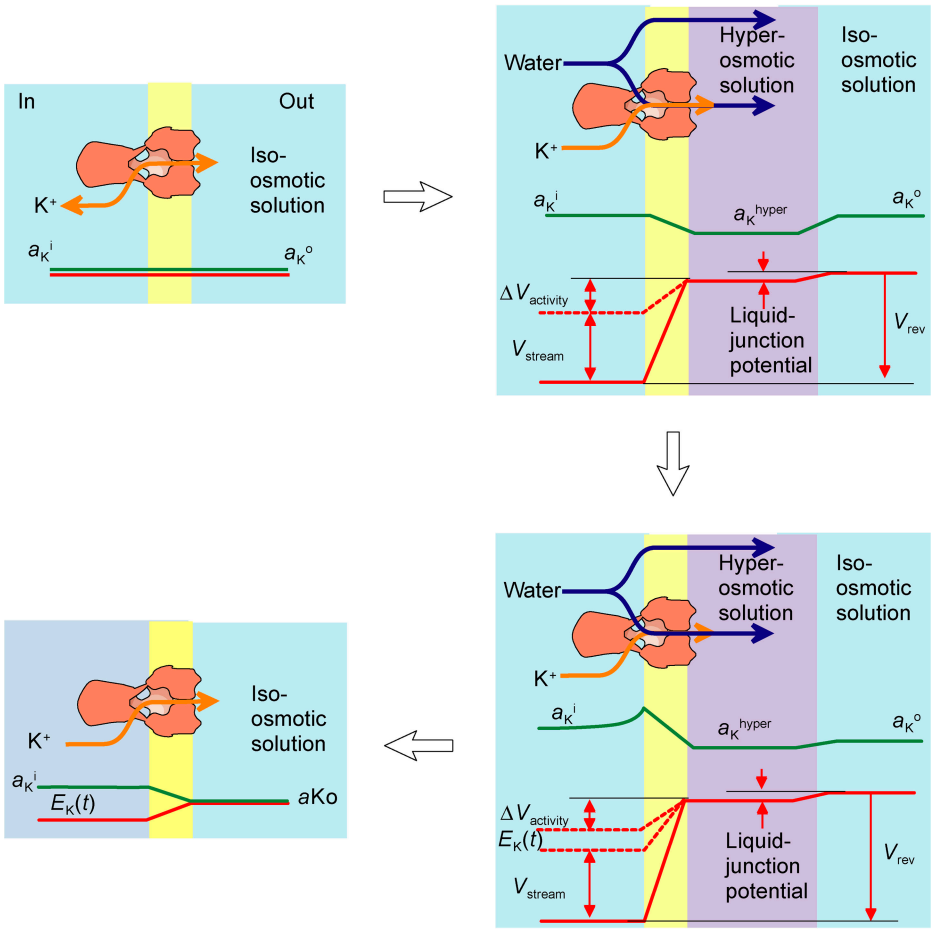

Figure 8. A scheme for potential profile around the channel. Lines indicate the concentration profile (green) and potential profile (red).

of secondary effects such as concentration polarization. Second, to avoid errors in evaluating V_{rev}, macroscopic current recordings were analyzed through fits with an equivalent membrane circuit. Even with fast ramp commands, nonlinear *I-V* curves were observed. This nonlinearity was optimized with the time-based changes in the membrane conductance. Our method gave accurate estimates of V_{stream} under various experimental conditions.

In our experimental configuration, some physicochemical factors, not considered in methods used previously, must be taken into account. The electrochemical profiles around the channel before, during, and after an osmotic pulse are summarized in Fig. 8. At the beginning (top left panel), the K^+ concentrations for the intra- and extracellular solutions were identical, leading to an E_K of zero. Upon the osmotic jump (top right panel), the changes in V_{stream} should be instantaneous, i.e., in the time range of the relaxation for ion permeation processes. Decreased activity of K^+ in the hyperosmotic solution altered the value of E_K across the K^+-selective membrane (E_K). In addition, at an interface between the hyperosmotic solution and isoosmotic solutions, differences in the activities of the constituent ions produced a liquid-junction potential, which was a unique outcome of our experimental configuration. These physicochemical potentials were evaluated separately (see MATERIALS AND METHODS) and subtracted from the measured shifts of V_{rev} upon the jump.

As the durations of the osmotic pulses were prolonged (Fig. 8, bottom right panel), the water efflux led to a buildup of K^+ in the cell. In the figure, both the local accumulation beneath the membrane (the concentration polarization) and the bulk accumulation are shown. These slowly developing factors were evaluated using the time course of the V_{rev} changes. A stepwise change followed by successive monitoring enabled the observations of these time-dependent events. Thus the measured shifts in V_{rev}, can be expressed as $V_{rev}(t) = V_{stream} + E_K(t) + \Delta V_{activity} + V_{LJ}$, where $E_K(t)$ includes local (beneath the membrane) and bulk changes in $[K^+]_i$. We conclude that the instantaneous shift of V_{rev} upon the jump represented the genuine V_{stream} and was free from the effects of secondary events, such as the concentration polarization.

In this study, V_{stream} was measured at symmetrical 10 mM K^+ concentration. From the V_{stream} value of 0.7 mV, the n value of 1.4 was obtained. This value was decreased significantly to 0.9 at symmetrical 100 K^+ solutions. This decrease is consistent with the previous reports (Levitt et al., 1978; Rosenberg and Finkelstein, 1978; Miller, 1982; Alcayaga et al., 1989; Dani, 1989; Tu et al., 1994; Ismailov et al., 1997; Tripathi and Hladky, 1998) and indicates increased occupancy of potassium ions in the pore. Recently the structural information of potassium channels has been accumulated and this information shed light on the interpretation of V_{stream}.

Crystal structure of several types of potassium channels revealed that the selectivity filter of these potassium channels has similar structure (Zhou et al., 2001; Jiang et al., 2002, 2003; Kuo et al., 2003; Long et al., 2005). With homologous sequence of the selectivity filter, HERG potassium channels seem not to be an exception. Then, what can we deduce from V_{stream} under the assumption of similar filter structure? The selectivity filter bears four sites each for either an ion or a water molecule. Among limited combinations of the occupancy states, mutual repulsion between K^+ ions would exclude the cases that K^+ ions sit in adjacent positions in the selectivity filter. Eight states remain and these are included in the shift-permeation model (Morais-Cabral et al., 2001). Therefore, the shift-permeation model can be considered as a general framework for permeation mechanisms of potassium channels, including HERG channels.

Fig. 1 C is a cycle flux diagram for the shift-permeation model, which shows how the coupling ratio is related to a permeation mode. This diagram is consisted with several cycles and by completing each cycle, ions and water molecules are transferred (cycle fluxes; Hill, 1989). In this diagram each cycle is accompanied with a water–ion coupling ratio (Levitt et al., 1978). Note that these coupling ratios are distinct and simple values (1,

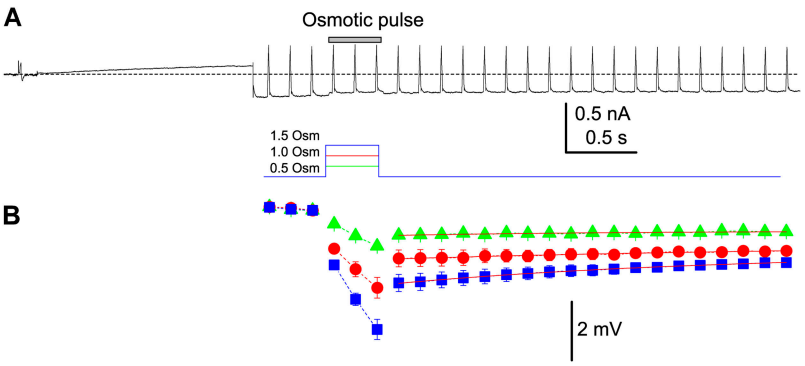

Figure A1. Time courses of the V_{rev} changes. (A) A current trace for a long train of ramps. A total of 25 ramps were applied at −20 mV. The osmotic pulse was applied from 4 to 6. (B) Time courses of V_{rev} for different osmotic pulses. V_{rev} values for each train were normalized by the value of prepulse (3). Time courses of recovery from the pulse (from 7 to 25) were fitted by a single-exponential function (red lines). The time constants were 1.5 s, 3.5 s, and 2.3 s for 500 mOsm, 1000 mOsm, and 1500 mOsm, respectively.

1.5, 2, or 3). Similar to the case that the net flux is a weighted sum of each cycle flux (Hill, 1989), the net coupling ratio should be a weighted sum of each coupling ratio. Thus, the experimentally obtained coupling ratio implies which cycle predominates and how each cycle is mixed to generate the total flux. The coupling ratio close to one ($n = 0.9$) obtained at 100 mM K^+ concentration may be represented by the cycle A (Fig. 1 C). Another possibility is that water molecules are able to slip past a K^+ ion near the beginning or end of the narrow pore (Levitt, 1984). These slippage transitions are indicated by broken lines in Fig. 1 B. For cycles with slippage transitions (those including three or four states in the top part of Fig. 1 B), the coupling ratios were calculated to be one. In either case, a K^+ ion in the midst of the selectivity filter is transferred with the least hydrated state. The cycle flux diagram with coupling ratios, which helps to relate V_{stream} and the permeation mode, is a useful tool to evaluate permeation models.

APPENDIX

The Time Course of V_{rev} Change after the Pulse

The values of V_{rev} after the osmotic pulse shifted significantly from those before the pulse. To investigate whether the shifts of V_{rev} were a transient phenomenon, a longer train of ramps was delivered, while the intracellular K^+ concentrations were monitored continually using V_{rev}. 19 ramps were applied after the osmotic pulse of 1,000 mOsm (Fig. A1, A) and the time courses of V_{rev} for three osmotic gradients were plotted (Fig. A1, B). After returning to the iso-osmotic solution, the recovery of V_{rev} was slow. The time courses of decay were fitted with a single-exponential function with a time constant of ~2 s, which is too long to be accounted for by dissipation of the locally accumulated K^+. Instead, the time for equilibration with the pipette solution seems to be more relevant.

We would like to thank G.A. Robertson for providing the HERG clone, and O.S. Andersen and A.F. James for critically reading the manuscript, F. Inoue for technical assistance, and T. Goto for secretarial assistance.

This work is supported by CREST of Japan Science and Technology Agency and Grant-in-Aid for Scientific Research from the Ministry of Education, Science, Sports, and Culture, Japan.

Olaf S. Andersen served as editor.

Submitted: 2 August 2005
Accepted: 10 October 2005

REFERENCES

Alcayaga, C., X. Cecchi, O. Alvarez, and R. Latorre. 1989. Streaming potential measurements in Ca^{2+}-activated K^+ channels from skeletal and smooth muscle. Coupling of ion and water fluxes. *Biophys. J.* 55:367–371.

Berneche, S., and B. Roux. 2001. Energetics of ion conduction through the K^+ channel. *Nature.* 414:73–77.

Chung, S.H., T.W. Allen, M. Hoyles, and S. Kuyucak. 1999. Permeation of ions across the potassium channel: Brownian dynamics studies. *Biophys. J.* 77:2517–2533.

Dani, J.A. 1989. Open channel structure and ion binding sites of the nicotinic acetylcholine receptor channel. *J. Neurosci.* 9:884–892.

Finkelstein, A., and O.S. Andersen. 1981. The gramicidin A channel: a review of its permeability characteristics with special reference to the single-file aspect of transport. *J. Membr. Biol.* 59:155–171.

Guidoni, L., V. Torre, and P. Carloni. 2000. Water and potassium dynamics inside the KcsA K^+ channel. *FEBS Lett.* 477:37–42.

Hille, B. 2001. Ion Channels of Excitable Membranes. Third edition. Sinauer Associated, Inc. Sunderland, MA. 814 pp.

Hill, T.L. 1989. Free Energy Transduction and Biochemical Cycle Kinetics. Springer-Verlag, Berlin. 119 pp.

Ismailov, I.I., V.G. Shlyonsky, and D.J. Benos. 1997. Streaming potential measurements in αβγ-rat epithelial Na^+ channel in planar lipid bilayers. *Proc. Natl. Acad. Sci. USA.* 94:7651–7654.

Jiang, Y., A. Lee, J. Chen, M. Cadene, B.T. Chait, and R. MacKinnon. 2002. Crystal structure and mechanism of a calcium-gated potassium channel. *Nature.* 417:515–522.

Jiang, Y., A. Lee, J. Chen, V. Ruta, M. Cadene, B.T. Chait, and R. MacKinnon. 2003. X-ray structure of a voltage-dependent K^+ channel. *Nature.* 423:33–41.

Katchalsky, A., and P.F. Curran. 1965. Nonequilibrium Thermodynamics in Biophysics. Harvard University Press, Cambridge, MA. 260 pp.

Kuo, A., J.M. Gulbis, J.F. Antcliff, T. Rahman, E.D. Lowe, J. Zimmer, J. Cuthbertson, F.M. Ashcroft, T. Ezaki, and D.A. Doyle. 2003. Crystal structure of the potassium channel KirBac1.1 in the closed state. *Science.* 300:1922–1926.

Levitt, D.G. 1984. Kinetics of movement in narrow channels. *Curr. Top. Membr. Transp.* 21:181–197.

Levitt, D.G., S.R. Elias, and J.M. Hautman. 1978. Number of water molecules coupled to the transport of sodium, potassium and hydrogen ions via gramicidin, nonactin or valinomycin. *Biochim. Biophys. Acta.* 512:436–451.

Long, S.B., E.B. Campbell, and R. Mackinnon. 2005. Crystal structure of a mammalian voltage-dependent Shaker family K^+ channel. *Science.* 309:897–903.

Luzhkov, V.B., and J. Aqvist. 2001. K^+/Na^+ selectivity of the KcsA potassium channel from microscopic free energy perturbation calculations. *Biochim. Biophys. Acta.* 1548:194–202.

Miller, C. 1982. Coupling of water and ion fluxes in a K^+-selective channel of sarcoplasmic reticulum. *Biophys. J.* 38:227–230.

Morais-Cabral, J.H., Y. Zhou, and R. MacKinnon. 2001. Energetic optimization of ion conduction rate by the K^+ selectivity filter. *Nature.* 414:37–42.

Rosenberg, P.A., and A. Finkelstein. 1978. Water permeability of gramicidin A-treated lipid bilayer membranes. *J. Gen. Physiol.* 72: 327–340.

Shimizu, H., C. Toyoshima, and S. Oiki. 2003. Interaction between tetraethylammonium and permeant cations at the inactivation gate of the HERG potassium channel. *Jpn. J. Physiol.* 53:25–34.

Tripathi, S., and S.B. Hladky. 1998. Streaming potentials in gramicidin channels measured with ion-selective microelectrodes. *Biophys. J.* 74:2912–2917.

Trudeau, M.C., J.W. Warmke, B. Ganetzky, and G.A. Robertson. 1995. HERG, a human inward rectifier in the voltage-gated potassium channel family. *Science.* 269:92–95.

Tu, Q., P. Velez, M. Brodwick, and M. Fill. 1994. Streaming potentials reveal a short ryanodine-sensitive selectivity filter in cardiac

Ca^{2+} release channel. *Biophys. J.* 67:2280–2285.

Zhou, Y., J.H. Morais-Cabral, A. Kaufman, and R. MacKinnon. 2001. Chemistry of ion coordination and hydration revealed by a K^+ channel-Fab complex at 2.0 Å resolution. *Nature.* 414:43–48.

Zhou, Y., and R. MacKinnon. 2003. The occupancy of ions in the K^+ selectivity filter: charge balance and coupling of ion binding to a protein conformational change underlie high conduction rates. *J. Mol. Biol.* 333:965–975.